Drafting of two passive swimmer scale models for open-water races

B Bolon, C Pretot, Christophe Clanet, Frédérique Larrarte, R Carmigniani

Drafting of two passive swimmer scale models for open-water races

Bolon B.[(1)], Pretot C.[(1)], Clanet C.[(2)], Larrarte F.[(1),(3)] & Carmigniani R.[(1)]

(1) LHSV, ENPC, EDF R&D, 6 Quai Watier, 78400 Chatou, France,(2) LadHyX, Ecole Polytechnique, Boulevard des Maréchaux, 92120 Palaiseau, France, (3) Université Gustave Eiffel, Cité Descartes, bâtiment Bienvenüe, 5 boulevard Descartes, Champs sur Marne, 77454 Marne la Vallée Cedex 2, France

baptiste.bolon@enpc.fr

1 Abstract

The interaction between two passive human swimmer scale models is investigated both experimentally and numerically. The Froude number, comparing the swimming velocity to the characteristic wave velocity, is conserved in the study. The interaction is quantified for a large range of relative positions and for 3 different speed corresponding to cruising, average and sprint swimming. The joined CFD study using OpenFoam allows us to determine the relative positions that optimise the drafting during an open-water race: just behind a lead swimmer or at the level of the hip of a neighbour, with reductions of drag of 40% and 30%, respectively.

2 Introduction and field observations

In nature, animals have learn to move, swim or fly in specific configurations in order to reduce the overall energy consumption of the pack [1, 2, 3]. For example, Weihs [1] showed that young dolphin calves keep up with their mother by swimming by their side. In this configuration, Weihs calculated that the calf could gain up to 90% of the thrust needed to move at the speed of its mother, thanks to both Bernoulli suction and the displacement effect. Also, some birds like geese or swifts are known to fly in V-formation.The energy saving obtained by flying in group increases their range of flight by 70% compared to a lone bird [2]. Similar conclusion exist for fish schooling: their endurance is increased by 2 to 6 times [3]. These situations are called drafting.

In sports, drafting is observed in team sports (team pursuit in cycling for example), or when racing against other athletes: running, swimming, car racing or cycling. The general idea is that an athlete can benefit from a drag reduction when being behind another one. Therefore the draft athlete produces less effort than their opponent to move at the same speed. This energy saving can make a difference in the outcome of a race. It exists in various disciplines as illustrated in figure 1. Drafting has been studied in various sports [4, 5, 6]. For example, in cycling, Blocken *et al.* [4] studied the drafting effect on 2 cyclists numerically,

highlighting the fact that the trailing cyclist encounters a reduction of his drag from 13% to 27% depending of his position on the bike and that this reduction decreases with distance.

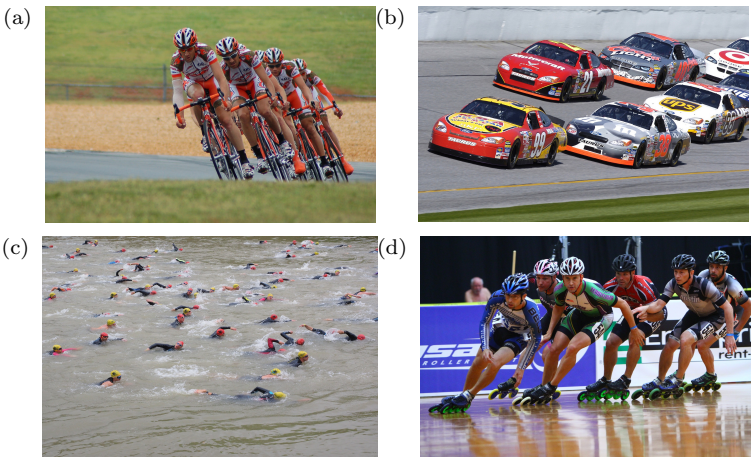

Figure 1: Examples of drafting situations in various sports, copyright-free pictures. (a) Peloton formation in cycling. (b) NASCAR racing. (c) Open-water swimming. (d) Speed skating.

Blocken *et al* [5] also measured drag on scale models in peloton formation thanks to wind-tunnel testing, showing that there are preferential positions in a peloton that allow a cyclist to encounter minimum drag. It is also a well-known phenomenon in racing cars. For instance, CFD studies in NASCAR (National Association for Stock Car Auto Racing) showed a drag reduction for the trailing car [6]. All previously mentioned sports are in air. In swimming, athletes move at the interface between two fluids: air and water, which makes drafting in swimming specific because of the waves created at this interface. Different studies have measured some physiological parameters and their evolution in drafting situations [7, 8, 9]. These articles draw the conclusion that drafting has a positive impact on physiological parameters such has a reduction of the concentration of blood lactate, a reduction in oxygen uptake and heart rate and a reduced perceived exertion on the Borg scale (which is a way of measuring physical activity intensity level based on physical sensations, [10]). As a consequence, draft swimmers will face less physical fatigue than isolated swimmers. Moreover, Janssen *et al.* [9] also shown a positive correlation between passive drag reductions in drafting formation and physiological benefit in active swimming in those same formations. There are also numerical papers that study drag forces and drag coefficients on passive swimmers [11, 12]. They suggest that the drafted swimmer encounters reduced drag compared to the leading swimmer, which can explain the evolution of physiological parameters mentioned before. The wave field created by a passive leading swimmer has been studied by Yuan & al. [13] using a potential theory approach and neglecting the wake produced

by the swimmers. They found that a draft swimmer following a leader could encounter a drag increase or decrease depending on the distance separating the 2 swimmers. This may be due to the transverse waves generated by the lead swimmer. Indeed, they are not disturbed by the turbulent wake which was neglected in the first place when choosing a potential approach. Finally, some works try to actually measure drag during drafting experimentally. For example, Westerweel [14] did some drag measurements on scale models and concluded that the drag reduction could be up to 40% for the draft swimmer. Our goal is to determine the relative positions of swimmers that allow them to make the most of drafting during open-water races. The study is conducted on passive scale models, which allows us to study a wide range of race configurations. First, we present our experimental and numerical set-ups. Then, we display our results for in line swimming and for side by side swimming.

3 Experimental and numerical setup

3.1 Experimental setup

All the experiments take place in the Electricité de France (EDF) Lab facility in Chatou, France. The scale models are fixed in an open water channel which is 80 meters long, 1.5 meter wide and 1.2 meter deep. A scheme of the whole facility is shown in figure 2.

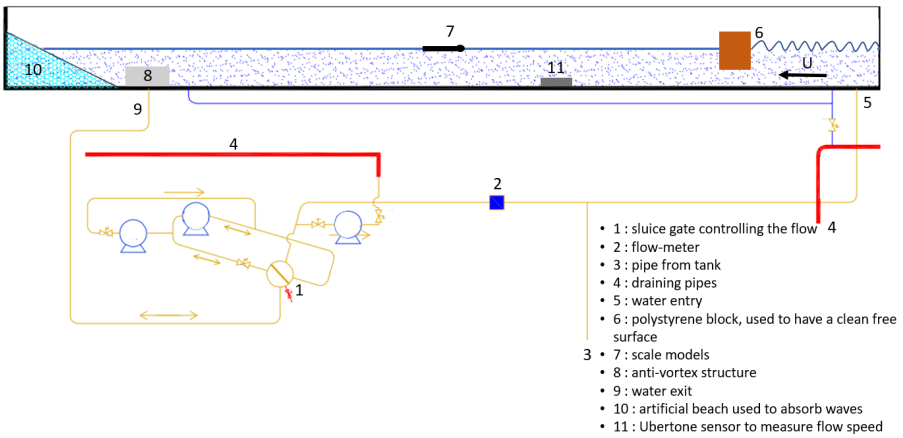

Figure 2: Schematic view of the flume in the longitudinal vertical plane.

The tank is filled with water up to an height $h = 0.7$ m (discussed later). The models position is controlled using a motored arm with millimetric precision. The model depth is fixed throughout the experiment. The position is chosen such that the swimmer head is just below the surface for the standing water case (no current in the tank) for repeatability. In this configuration, the swimmer shoulders are slightly out of water. Once the pump is running the water height

increases slightly (about 2 cm). In running configuration, the swimmer is then fully submerged. We use an anti-vortex structure at the water exit in order to prevent air from penetrating the pump. We choose to study 3 different speeds of the flow, in order to represent different swimming paces characteristic of open water races. These speeds are 1.25, 1.5 and 1.7 m/s for human swimmers. In the following, they are respectively called cruising, average and sprint speeds. To determine the corresponding speed of the flow in the flume for our scaled experiment, we use a Froude similitude:

$$Fr = \frac{V}{\sqrt{gL}}, \tag{1}$$

with V the velocity of the flow, g the gravity constant and L the length of a swimmer. We obtain $Fr = 0.28, 0.34$ and 0.38 for the 3 swimming speeds chosen respectively, using 2 m as the length of a human swimmer. We work in the deep-water limit to mimic conditions encountered by actual swimmers in races. We note k the wavenumber of the transverse waves created by the scale model. We have $k = 2\pi/\lambda$ where λ is the wavelength. According to [15], we are in a deep-water regime if $kh >> 1$, where h is the water height. The order of magnitude of λ will be the length of the scale model. Since the maximum flow in the flume is 1000 L/s, we choose the length of our scale models to be 0.4 m and the water depth to be 0.7 m, in order to fulfil both Froude numbers conditions and deep-water constraint. Knowing the length of our model, we determine the speeds of the flow in our flume thanks to the Froude similitude. They are 0.56, 0.67 and 0.75 m/s. We can then calculate the Reynolds number of our flow, defined as:

$$Re = \frac{VL}{\nu}, \tag{2}$$

where ν is the water kinematic viscosity. For the smallest speed, we obtain $Re = 2.24 \times 10^5$. For human swimmers, taking $L = 2$ m and $V = 1.5$ m/s (typical open water swimming speed), we obtain $Re = 3 \times 10^7$. Both are large enough to assume that a turbulent regime is reached. Details about Reynolds independence of the drag coefficient are provided in Appendix C. A close view of the setup is shown on figure 3.

Models are 3D printed, using PLA (polylactic acid) and using a 0.0004 m diameter nozzle. The geometry of the model is available as supplementary material [16]. Drag forces are measured using 1D-shear force sensors designed by *Phyling* [17]. They are shown in figure 3, as items 3 and 4. The force measured with the sensors goes from 0.2 N to 0.9 N depending on the configuration studied. Details are provided in Appendix B. Drag is acquired at 100 Hz during 20 seconds, repeated 6 times and averaged for each configuration studied. Speeds are measured with a UB-flow acoustic profiler from Ubertone. Velocity measurements were made to assess velocity variation in the z-direction and y-direction. They are shown in figure 4. From the profile made along the transverse axis, we deduce that the flow speed remains constant in the measurement zone (delimited the 2 red horizontal lines). The asymetry of the profile can be explained by the

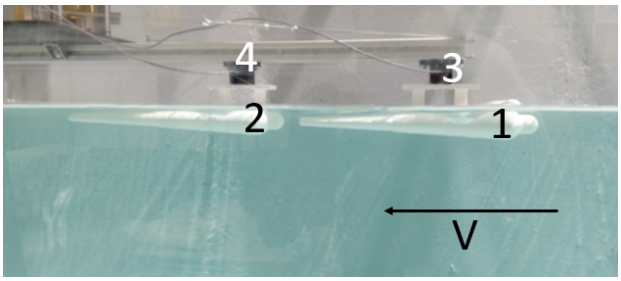

Figure 3: Experimental setup. (1) Lead scale model, (2) Draft scale model, (3) and (4) 1D-shear force sensors

fact that one side of the flume is a rough wall, while the other side is made of smooth glass.

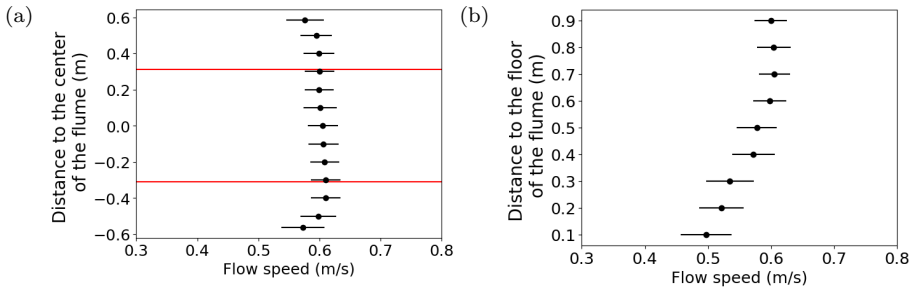

Figure 4: Streamwise velocity profile in the flume for a given flow. (a) Profile along the transverse axis of the flume. (b) Profile along the vertical axis of the flume.

Forces convention are presented in figure 5. F_x stands for the force in the direction of the flow, i.e drag force. F_y stands for the force in the perpendicular direction to the flow, in the plane of the water surface, i.e side force. Finally, F_z stands for vertical force. In this work, we focus on drag and side forces.

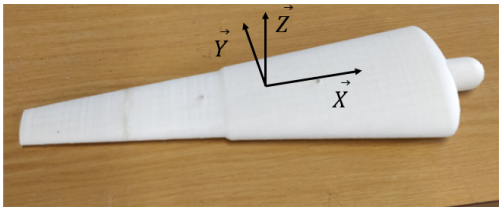

Figure 5: Frame of reference.

3.2 Numerical method

Numerical studies are done using OpenFoam software v2012 [18] and *interFoam* solver (which uses a Volume Of Fluid method (VOF)). A mesh is created thanks to the *blockMesh* command. The domain is 12m long, 2m large and 5m high. Six refinement boxes are used to refine the mesh in the regions of the scaled models, thanks to *topoSet* and *refineMesh* commands. Finally, the scale models' geometry is exported into the mesh with the *snappyhexMesh* command. A zoomed view of the mesh around a model is displayed in figure 6.

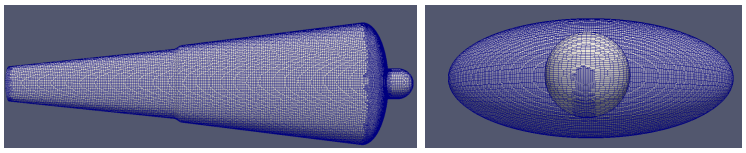

Figure 6: Zoomed view of the mesh around a model.

A speed is imposed at the inlet of the mesh in order to recreate the conditions of our experiment. On the side, bottom and top faces of the domain, a wall condition is imposed. At the outlet, a *zeroGradient* pressure condition is imposed. We use a k-ω SST turbulence model: a blending function activates either the Wilcox model near walls or the k-ϵ model in free stream, which ensures that the appropriate model is used for the entire flow field. The parameters used for this turbulence model are those of the OpenFoam documentation [19]. Fluids are considered incompressible. For water, we use $\rho = 998.8kg/m^3$ and $\nu = 1 \times 10^{-6}m^2/s$. For air, we use $\rho = 1.2kg/m^3$ and $\nu = 1.5 \times 10^{-5}m^2/s$. The time step used is dt = 0.01s for lowest speeds and 0.001s for the higher speed to ensure convergence. There are approximately 4 millions cells in our OpenFoam cases. Each case represents 36 hours/CPU. To assert convergence, we looked at the evolution of the drag force computed at each iteration by OpenFoam. An example is shown in figure 7. Moreover, at each time step we make sure that both pressure and alpha (volume of water in each cell) had converged. This is made by looking at the value of residuals in OpenFoam. To assert spatial convergence, we performed different cases with different mesh cells sizes.

4 Results

4.1 In line swimming

4.1.1 Measurements

For in line swimming, we define L_x as the distance between the head of the 2 models. Considering that the frame of reference, defined in figure 5, is attached to the lead scale model, L_x is negative in this section and $L_x/L < -1$ to ensure there is no collision between models. The definitions and conventions are shown in figure 8a. We introduce the drag coefficient of a lone swimmer as :

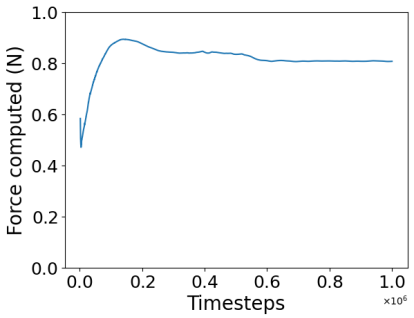

Figure 7: Evolution of the drag force computed during a CFD simulation.

$$C_{d,0} = \frac{F_x}{\frac{1}{2}\rho S V^2}, \tag{3}$$

where F_x is the drag force, ρ is the water density, S is the frontal area of a swimmer and V the speed of the flow. The values of $C_{d,0}$ are 0.58 ± 0.052, 0.62 ± 0.056 and 0.60 ± 0.054 for $V = 0.56, 0.68$ and 0.75 m/s respectively. We also define the normalised drag as:

$$\overline{C_d} = \frac{C_d}{C_{d,0}}, \tag{4}$$

where C_d is the drag coefficient measured during the in-line swimming experiment. With this definition, a configuration where $\overline{C_d}$ is smaller than 1 is advantageous for the swimmer compared to swimming alone, and disadvantageous if it is higher than 1. The experiment consists in measuring drag for the lead and draft scale models, for a wide range of L_x and for the 3 speeds chosen in the previous section. The results displayed in this section on figures 8b, 8c and 8d are the evolution of the normalised drag with the non-dimensional distance between models for both the leading model and draft model. We show both lab measurements and OpenFoam results. The error bar stands for the 95% reliability interval.

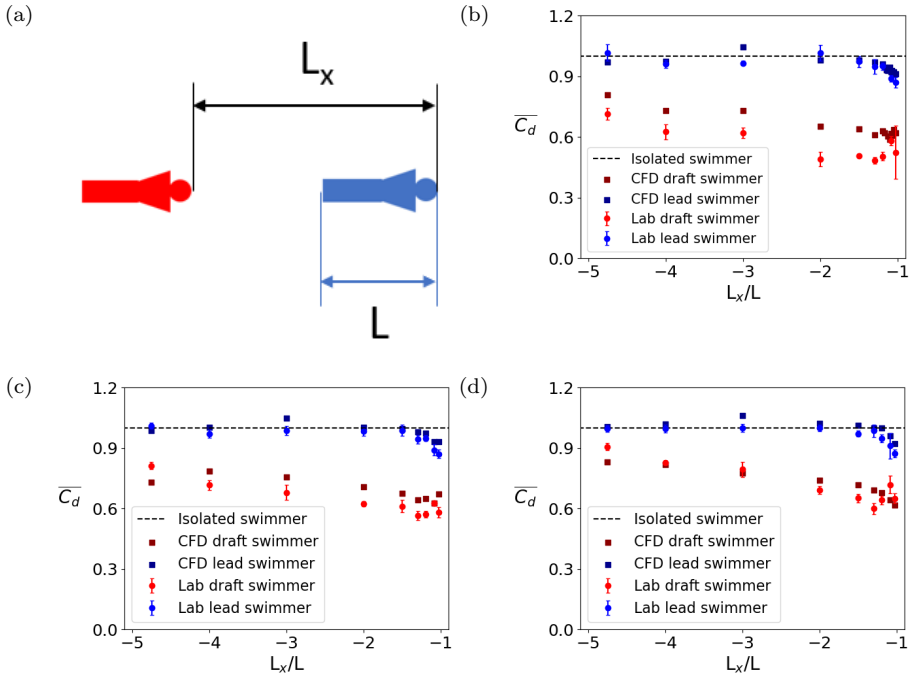

Figure 8: Drag measurements for 3 different Froude numbers for in line swimming. (a) Schematic view of in-line swimming set-up. (b) In line swimming results for Fr = 0.28. (c) In line swimming results for Fr = 0.34. (d) In line swimming results for Fr = 0.38.

For the leading model, our results show that it encounters a drag reduction, up to 15%, when closely followed by another one. Quantitatively, its normalised drag is smaller than 1 for non-dimensional distances in the interval [-1.5, -1]. That is to say when it is followed at less than half a body length. For the draft model, our measurements show a big reduction of its drag, up to 45% in some configurations, when located right behind the leader. Then, the reduction of drag decreases as the distance between models increases. However, the reduction of drag still exists at 4 body lengths behind the leader : 30%, 20% and 10% reductions for $Fr = 0.28, 0.34$ and 0.38 respectively. These results are similar to those reported in previous studies in various sports: [4, 11, 14].

4.1.2 Discussion about the results, free surface analysis

In the experimental results, shown in figures 8b, 8c and 8d, a systematic increase of drag is noticeable for the second closest position for the draft model. This corresponds to the position $L_x/L = -1.0875$ and is outlined by the vertical red line in figure 9. This fluctuation in the drag reduction of the drafter is not observed for fully submerged models in other sports and might be due to

the presence of the interface between the two fluids. This fluctuation of drag reduction for the drafter appears to be similar to the wave effect reported by Yuan *et al.* [13] in their potential approach. The free surface deformation, ζ, for a lone scale model along the $y = 0$ axis was computed using OpenFoam and is shown in figure 9. The free surface deformation shows a negative gradient ahead of the swimmer similarly to [13]. Behind the swimmer, we can see a single bump with a maximum near $L_x/L = -1.0875$. This wave positive gradient in the x-direction might explain the increase in drag observed in this configuration. However, some of our results are in discordance with [13], for both drag measurements and free surface state. Indeed, [13] highlights that for in line swimming, there is an alternance of positions with reduction of wave drag and positions with increase of wave drag depending on the value of L_x, whereas in our experiments all the configurations studied show a drag reduction for the draft scale model. Concerning free surface, [13] shows a transverse wave region, whereas in our case, there is only one significant wave behind the scale model because of its turbulent wake. Those differences may be due to the potential approach chosen by [13], when both our experiments and CFD simulations are in a turbulent regime, which is closer to reality for human swimmers.

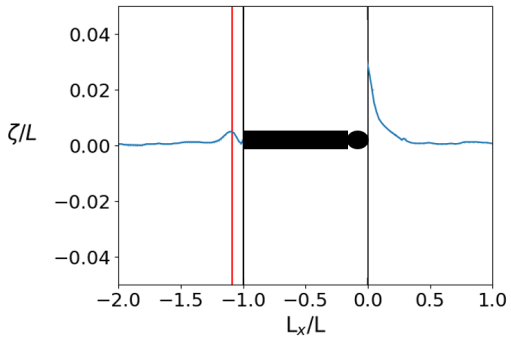

Figure 9: Free surface profile, lone scale model, Fr = 0.28

4.2 Side by side swimming

4.2.1 Drag forces

During open-water races, swimmers are often side by side either to pass an opponent, swim around a turn buoy or at the feeding station. Moreover, it is simpler for them to see where they are going when side by side, in order to follow a bee-line between turn buoys. That is the reason why we also study side by side swimming configurations. The experimental setup is shown on figure 10. We define L_x as the distance between the 2 heads of our models in the direction of the flow and L_y as the distance between the 2 heads in the direction perpendicular to the flow, as described in figure 11a. With this definition, the minimum value of L_y is 12 cm as models are 12 cm large at the shoulder level.

In the first set of experiments, L_y remains constant: $L_y = 12.5$ cm, whereas L_x varied. We chose this value for L_y as it is the minimum reachable value, taking into account that actual swimmers cannot swim too close from each other due to their arms moving. The influence of L_y is studied in the next sections.

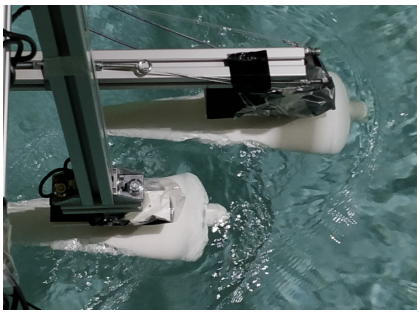

Figure 10: Side by side swimming setup, top view.

In figures 11b, 11c and 11d we present the evolution of normalised drag (defined as in equation 4) with non-dimensional distance L_x/L. For instance, a non-dimensional distance L_x/L of 0 means that scale model are perfectly side by side, and -1 means that the head of one model is at the feet of the other one. Moreover, a non-dimensional distance L_y/L of 0.3 means that models' shoulders are touching, and a greater value means that models do not touch each other. We show results from both lab experiments (blue dots) and OpenFoam results (black squares). The error bar stands for the 95% reliability interval. We notice that for the 3 speeds, the normalised drag is maximum when models are aligned with no gap (meaning L_x=0). Moreover, this maximum does not seem to be affected by the speed: indeed, it stays between 1.25 and 1.3 for the 3 speeds. As the normalised drag is higher than one, that means that in this configuration, scale models encounter a drag larger than the one they experience alone. As a consequence, in a race, swimmers should avoid this side by side configuration if they want to preserve their physical strength and reduce fatigue. However, they can also try to impede the passing of an opponent and wear them out by blocking them in this configuration. We can also observe, for each speed, a minimum of drag. This minimum happens for a non-dimensional distance between -0.3 and -0.5, meaning that the measured model is at the hip of its neighbour. Contrary to the maximum of drag, the value of the minimum depends of the speed of the flow. It's equal to 0.9, 0.8 and 0.7 respectively for $Fr = 0.28, 0.34$ & 0.38. Those value of the normalised drag highlights that this position is the best for swimmers who want to save their energy and cannot swim in line. Moreover, we can see that the minimums of drag for side by side swimming are higher than the minimums for in line swimming. If swimmers have the choice and want to preserve themselves, they should thus swim in line behind a leader. Finally, we observe that lab data and CFD data match pretty well: the same phenomenons occur at the same locations and with the same intensity.

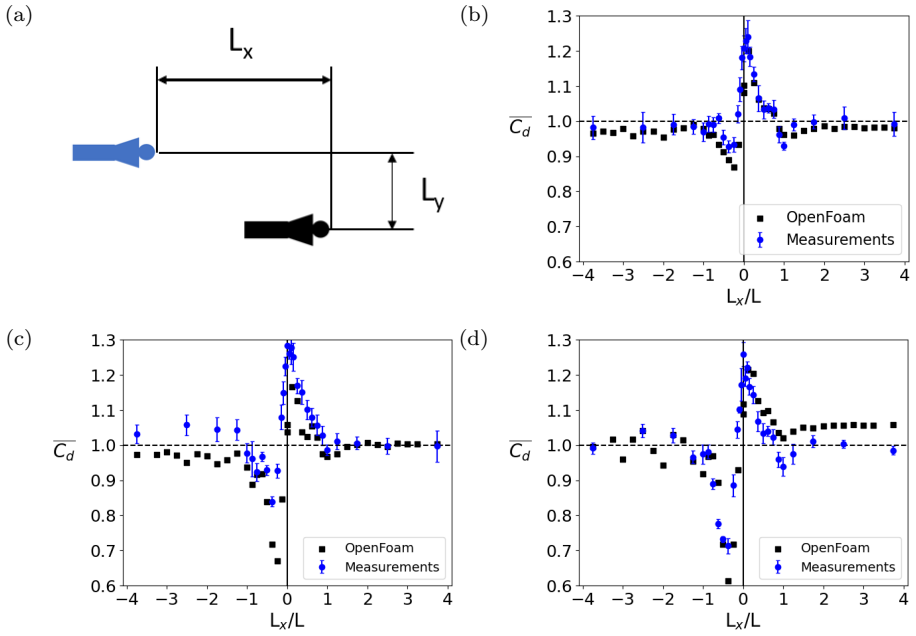

Figure 11: Drag measurements for 3 different Froude numbers for side by side swimming with $L_y/L = 0.3125$. (a) Schematic view, side swimming. (b) Side swimming results for Fr = 0.28. (c) Side swimming results for Fr = 0.34. (d) Side swimming results for Fr = 0.38

4.2.2 Force map

For each speed, and for different values of L_y ($L_y/L \in [0.3125, 0.375, 0.45, 0.6, 0.9, 1.2]$), we perform drag measurements, as we did in the previous section. The aim here is to characterise the drag force encountered by the scale model in a 2D-space, in order to have a better understanding of the positions that could be advantageous or disadvantageous. We also extend our CFD study with OpenFoam to configurations not studied experimentally. Our results are shown on figure 12. The black contour is a schematic view of one model. The grey zone represents the part of the 2D space where the model cannot be without overlapping its neighbour. Each dot represents a measurement point and is the location of the scale model's head relatively to the black model on the graph. The colour of the dot represents the intensity of the drag force. Each figure is divided in 2 parts: the top part (discrete points) is lab measurements and the bottom part (continuous data) is the OpenFoam results and interpolation.

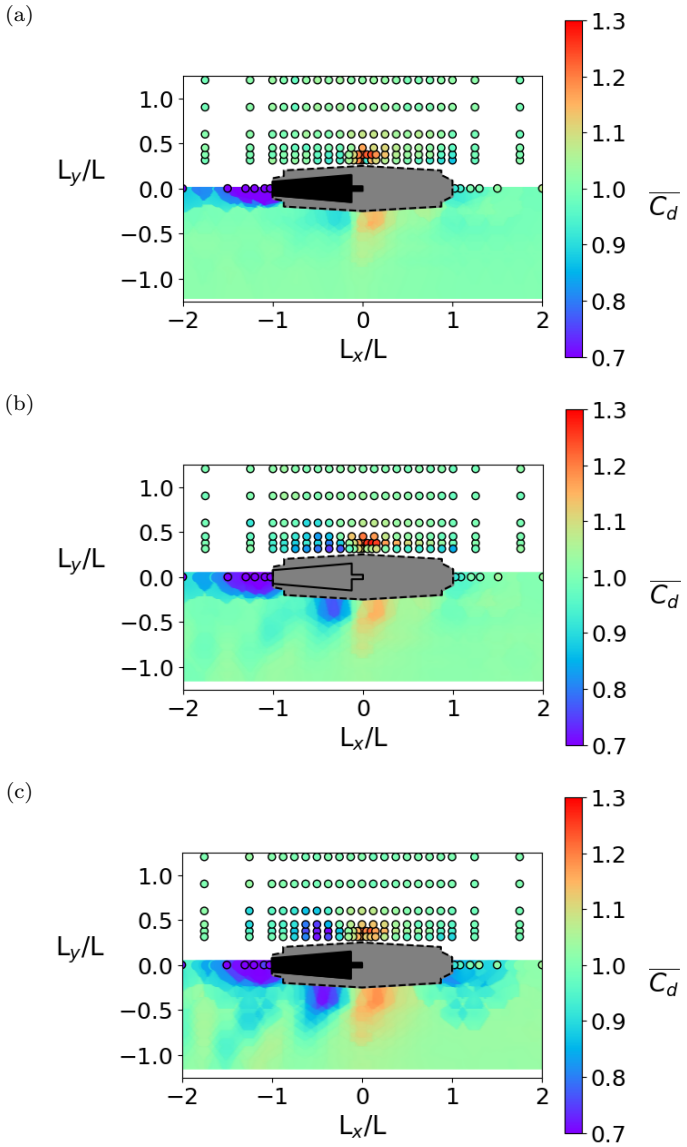

Figure 12: 2D-map of the drag, comparing lab and CFD data. (a) 2D drag map for Fr = 0.28. (b) 2D drag map for Fr = 0.34. (c) 2D drag map for Fr = 0.38.

Firstly, we observe that the location of the advantageous and disadvantageous configurations seem to be independent from the speed of the flow. We also notice that, when $L_y/L > 0.75$ (meaning when the lateral distance between models is more than 3 quarters of a body length), there is no more drafting phenomenon

as the model's drag coefficient is equal to the one of an alone model. This confirms that the best configuration to encounter a minimal drag is to swim right behind the feet of a leading swimmer, or to be at the hip of an opponent. The worst configuration, where the drag is maximum, is when swimmers are perfectly side by side.

4.2.3 Free surface analysis

Using OpenFoam simulations, we are able to plot the free surface of the flow, for a lone scale model. The results are shown in figure 13a and can be qualitatively compared to the experiment in figure 13b. Comparing the free-surface height with the advantageous and disadvantageous configurations highlighted in figure 12, we can say that, for side swimming, reductions of drag seem to be mainly due to swimming on a negative gradient, projected in the x-direction, wave. This can be confirmed by looking at a free-surface profile for a chosen value of L_y. An example is shown on figure 14. We plotted the head position for the maximum (grey vertical line) and the minimum of drag (black vertical line). We observe that for the minimum of drag, a large part of body is facing a negative gradient, projected in the x-direction, wave: the model is 'surfing' the wave created by its neighbour, which explains the reduction of drag measured both in lab and CFD. On the opposite, for the maximum of drag, the model is facing both positive and negative wave gradient, projected in the x-direction. As a consequence, the increase of drag does not come solely from wave gradient. We can explain the increase of drag when models are close to each other: the wave created by each model in its upstream, as seen next to the head in figure 13a, interacts to create a bigger wave. We suppose this, as a consequence, increases the wave drag of both models and therefore increases their total drag.

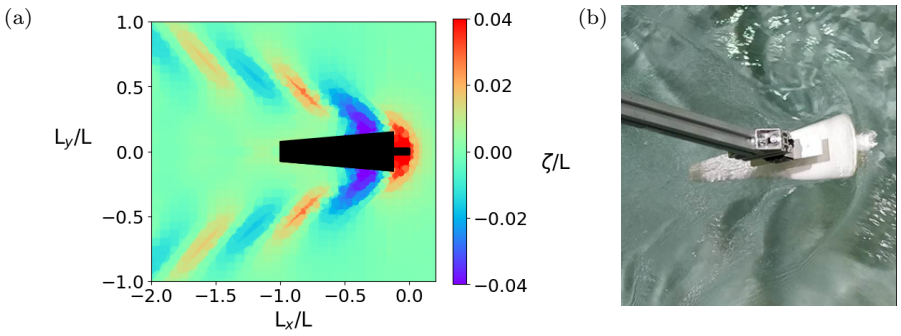

Figure 13: (a) Free-surface height for Fr = 0.34, obtained with OpenFoam. (b) Qualitative experimental wavefield for Fr = 0.34

To confirm or reject our assumptions about the influence of free surface, we complete our work by computing 3 different fully submerged cases: an alone model, 2 models head to head corresponding to the maximum of drag found in figure 11 with $L_y/L = 0.3125$ and 2 models with one at the hip of the other

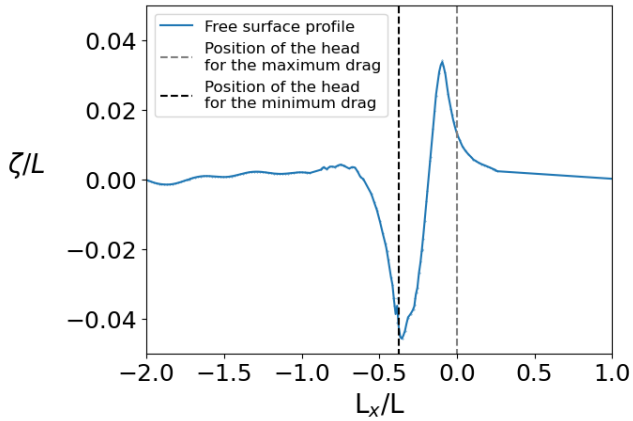

Figure 14: Free-surface height for Fr = 0.34, $L_y = 0.015$ m, obtained with OpenFoam.

with $L_y/L = 0.3125$ and $L_x/L = -0.4$, corresponding to the minimum of drag found in figure 11. For each case, we compute the normalised drag (the drag divided by the drag of an alone and fully submerged model).

Case studied	Normalised drag
Alone model	1.000 ±0.008
Side by side model	1.015 ±0.006
Hip lead model	1.033 ±0.004
Hip draft model	1.023 ±0.009

Table 1: Results for CFD fully submerged cases.

The results shown in table 1 highlight the fact that we do not have anymore the variations of drag observed for the free surface case. Moreover, the drag force encountered by the models are roughly the same for all the submerged cases studied and equal to the drag of an alone submerged model. This confirms that the variations of drag shown in figure 11 and 12 can be explained by waves and free surface effect in our work.

4.2.4 Side forces

To quantify side forces, we use the same sensors as for drag forces measurements. We use the following convention: a positive force means that the scale model studied is repulsed by its neighbour and a negative force means it is attracted by its neighbour, as described on figure 15a. We define the side coefficient as:

$$C_s = \frac{F_y}{\frac{1}{2}\rho S V^2}. \tag{5}$$

We also define the normalised side coefficient in the same way as for the normalised drag coefficient:

$$\overline{C_s} = \frac{C_s}{C_{d,0}}. \tag{6}$$

Results are displayed on figure 15b.

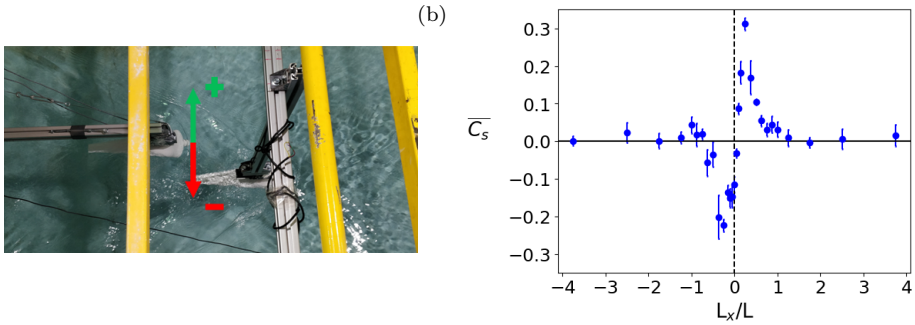

Figure 15: Side forces measurements for Fr = 0.38 and L_y/L = -0.3125. (a) Side forces conventions. (b) Lab results.

We observe that when a model is slightly in front of another one, it encounters a positive transverse force, which means it is repulsed by its neighbour. Moreover, when one is slightly behind another model, it encounters a negative transverse force, meaning it is attracted by its neighbour. If we look at the configuration shown in figure 15a, we conclude that both models will encounter a force which drags them towards their right. As a consequence, even if transverse forces are low compared to drag forces, swimmers will still have to compensate in order to swim in a straight line, which is crucial in open-water swimming in order to use a beeline between two turn buoys.

4.2.5 Evolution of drag with lateral distance L_y.

To quantify the interaction zone between swimmers, we decided to study numerically the influence of the lateral distance between models noted L_y as defined in 11a. For this study, models are perfectly side by side ($L_x = 0$) and we only change L_y separating them. Results are shown on figure 16. As shown on the graph, when models are really close to each other, drag is maximum. Then, as the lateral distance between them increases, the drag they encounter decreases, to finally reach a stable value for great distances, that is to say more than 0.75 body length. This may raise the idea that one should move aside when passing an opponent in order to reduce the encountered drag.
Moreover, the blue vertical line represents the position of the swimming-pool lane if both swimmers are located at the exact centre of their swimming lane, which represents a distance of 2.5 m in real life. This might justify the empirically chosen width of a swimming lane in competitions. Moreover, it outlines the crucial role of swimming lanes ropes in competition.

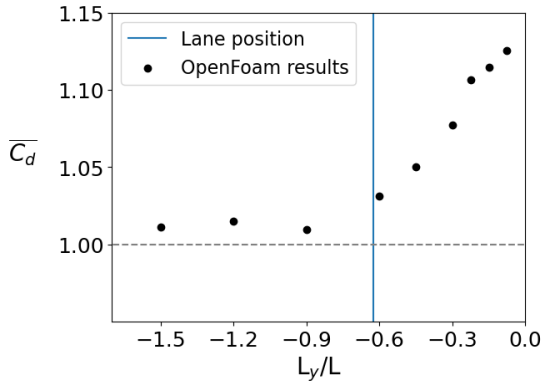

Figure 16: Influence of lateral distance on drag for Fr = 0.38, $L_x/L = 0$, results obtained with OpenFoam.

5 Conclusion

We used laboratory measurements on scale models to study drafting in both in line and side by side swimming. We observe that the best configuration to benefit from drag reduction in a 2 swimmers configuration is to follow as closely as possible a leading swimmer. Moreover, being at the hip level of an opponent is also a great way to encounter a reduction of drag, by riding the wave created by the opponent. On the contrary, being at the head level of an opponent makes both swimmers encounter a maximum drag, superior to one's of an isolated swimmer. The CFD simulations confirm the experimental results and allow us to extend the study to quantify the region of interaction between swimmers. There is a good correlation between CFD results and lab measurements. CFD also helped us to explain phenomenons observed during experiments thanks to free-surface analysis. However, the impact of active swimming on our drag measurements is still unknown and will have to be studied in a future work. We also need to study peloton configurations, as they often occur in open-water races.

Appendix A: Comparison with a buoyant case

To evaluate the effect of buoyancy, we compare our results to those of Westerweel *et al.* [14]. Indeed, our models are not free to move on the vertical axis, whereas it was possible in Westerweel *et al.*'s work for one model when the other one was fixed.

The setup is very similar to our setup: scaled models are placed in a flume which is 3 meters long and 1.5 meter wide. We work at the same Froude number, $Fr = 0.28$. There are slight geometry differences between our scaled models and those used here. Moreover, in this study, contrary to ours, models are buoyant and therefore can move along the vertical axis which is closer to real human swimmers. This setup is shown on figure 17a.

The comparison between non-buoyant and buoyant cases is shown on figure 17c. On this graph, non-buoyant results are the square points and the crosses are buoyant results. For the leader (blue squares and black crosses), we observe the same phenomenon. The leader encounters a drag reduction when closely followed by an opponent. This reduction is about 10% and seems to not be affected by buoyancy. For the draft model (red squares and grey crosses), we both observe a big drag reduction, but it is more important in the buoyant experiment: 55% versus 45% in our case. This difference can be explained by an increase of the uplift of the draft model. As a conclusion, we found similar results for the lead model and less drag reduction than Westerweel for the draft model. The model of a completely buoyant swimmer may be a little exaggerated and as a consequence the uplift bigger than for an actual swimmer. So, the drag reductions may be over-evaluated. However, the truth may be found in between our experiments and his, as we observe the same tendencies and physical phenomenons.

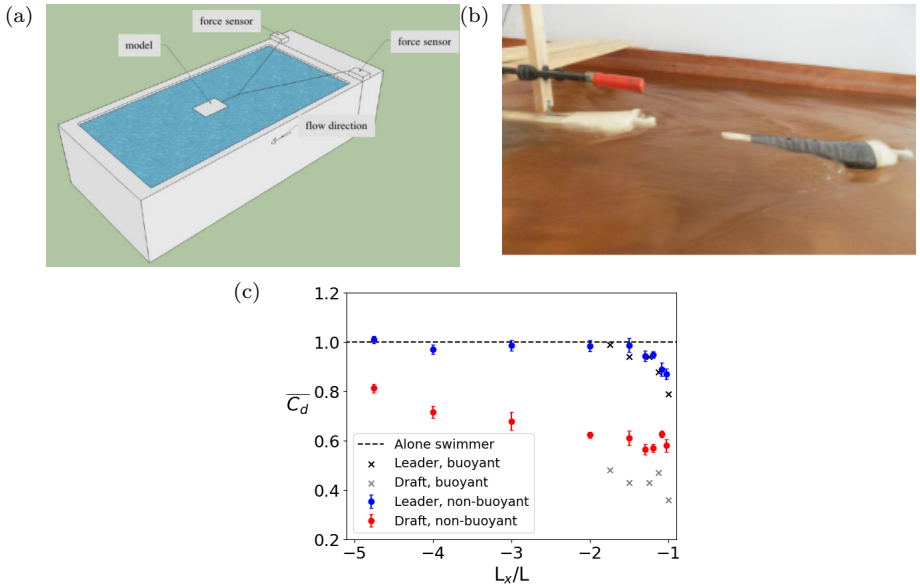

Figure 17: Comparison with Westerweel's buoyant case [14]. (a) Westerweel's experimental setup. (b) 2 scale models setup. (c) Comparison of the results, Westerweel & al data extracted from [14].

Appendix B: Multivariate error analysis

In this section, we define u as the measurement error and U as the 95% reliability interval. We therefore have $U = 2u$. We also define the drag coefficient as in Equation 3. The force F is obtained by multiplying the tension A measured by

the sensor with a constant conversion coefficient k. Moreover, the frontal area S is an ellipse, meaning we have $S = \pi ab$, where a and b are the half of big and small axes of the ellipse. Therefore, the drag coefficient is obtained as follows:

$$C_d = \frac{kA}{\frac{1}{2}\rho\pi abV^2} \tag{7}$$

We can then apply the formula for error propagation:

$$\frac{u(C_d)}{C_d} = \sqrt{(\frac{u(k)}{k})^2 + (\frac{u(A)}{a})^2 + (\frac{u(\rho)}{\rho})^2 + (\frac{u(a)}{a})^2 + (\frac{u(b)}{b})^2 + (\frac{u(V^2)}{V^2})^2} \tag{8}$$

Then, we have a look at each term of the right member:

- Concerning k. k is the coefficient which converts the tension measured by the force sensor in Volts into a force in Newtons. The sensors have a range of -5N to 5N. To obtain k, for both sensors, we perform a calibration before the beginning of the experiments. This consists in suspending various known masses to the sensor (fixed to the swimmer as in the experiment) using a pulley. An example of calibration's result is shown bellow:

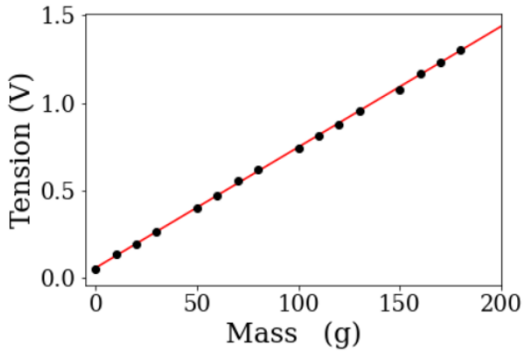

Figure 18: Results of sensor calibration: tension obtained for different suspended masses.

We obtain for the 2 different sensors, $k_1 = 1.239$ N/V, $u(k_1) = 0.0095$ N/V , $k_2 = 1.424$ N/V, $u(k_2) = 0.02$ N/V .

- Concerning A. A is the mean tension measured during 6 trials of 20 seconds . Then, $u(a)$ is obtained by computing the standard deviation of the mean tension signal. A and $u(A)$ depend on the trial and are computed for each trial.

- Concerning ρ. Water in the flume is at ambient temperature, that is to say between 15 and 20°C. We have ρ(T=15°C) = 999.77 kg/m3 and

ρ(T=20°C) = 998.29 kg/m3. Considering a uniform distribution of temperatures during the various trials, the mean value is ρ = 999.03 kg/m3 and u(ρ) = U(ρ)/2 = 0.37 kg/m3.

- concerning a. $a = 0.06$ m in the stl file. According to the properties of the 3D printer (RAISE 3D Pro2 Plus), we have $u(a) = 10\mu m$. This is independent from the trial.

- concerning b. $b = 0.025$ m in the stl file. According to the properties of the 3D printer (RAISE 3D Pro2 Plus), we have $u(a) = 10\mu m$. This is independent from the trial.

- Concerning V^2. Firstly, we use that $\frac{u(V^2)}{V^2} = 2\frac{u(V)}{V}$. Speed was not measured at each trial, but each time flow speed was changed in the flume. Therefore, for each aimed speed we give a mean value and U the 95% reliability interval given by the standard deviation of all the speeds obtained for one aimed speed. For V aimed at 0.56m/s: V = 0.561m/s and u(V) = 0.005 m/s. For V aimed at 0.67m/s: V = 0.678 m/s, and u(V) = 0.006 m/s. For V aimed at 0.75m/s: V = 0.750 m/s, and u(V) = 0.006 m/s.

We compute the multivariate error for one given example: a trial of a single swimmer at 0.56m/s. We obtain $\frac{u(C_d)}{C_d} = 0.045$. For this trial, we have $C_d = 0.580$. Moreover we use that $U(C_d) = 2u(C_d)$. Finally, we obtain: $C_d = 0.580 \pm 0.052$

Appendix C: Evolution of the drag coefficient with the Reynolds number.

As stated in section 3.1, at the smallest speed studied, for our scale models, we have: $Re = 2.24 \times 10^5$. Whereas for human swimmers, we have $Re = 3 \times 10^7$. Therefore, we have to make sure that the drag coefficient is independent from the Reynolds number if we want to generalise our results to human swimmers. We performed CFD calculations on a fully submerged scale model using OpenFoam as presented in section 3.2. We changed the speed of the flow several times to change the Reynolds number. We chose to make this study using CFD as it allows us to explore a wider range of flow speeds compared to lab measurements. The results are shown on figure 19. We observe that the drag coefficient remains roughly constant for $Re \in [1.2 \times 10^5; 1 \times 10^7]$. Therefore, our results can be generalised to human swimmers. Moreover, for a smaller Reynolds number : $Re = 3.6 \times 10^4$, there is an increase of the drag coefficient, which may be the sign of the drag crisis. However, no measurements or CFD calculations were performed at such low Reynolds number.

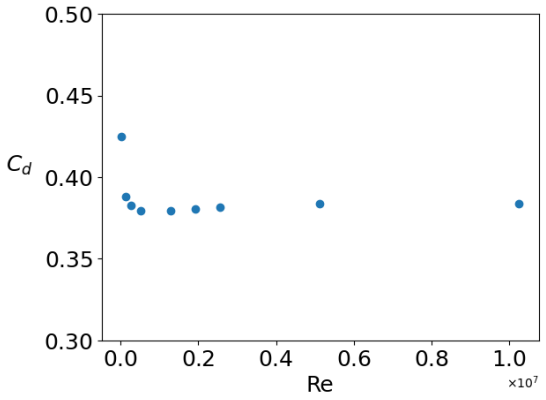

Figure 19: Variation of the drag coefficient with the Reynolds number.

References

[1] Weihs D, *The Hydrodynamics of Dolphin Drafting*, Journal of Biology, 2004, https://doi.org/10.1186/jbiol2

[2] Lissaman PBS and Shollenberger CA, *Formation Flight of Birds*, Science, Volume 168, Number 3934, Pages 1003-1005, 1970, 10.1126/science.168.3934.1003

[3] Weihs D, *Hydromechanics of Fish Schooling*, Science, Volume 241, Number 5387, Pages 290-291, 1973

[4] Blocken B, Defraeye T, Koninckx E, Carmeliet J & Hespel P, *CFD Simulations of the Aerodynamic Drag of Two Drafting Cyclists*, Computers and Fluid, Volume 71, Pages 435-445, 2013

[5] Blocken B, van Druenen T, Toparlar Y, Malizia F, Mannion P, Andrianne T, Marchal T, Maas GJ and Diepens J, *Aerodynamic drag in cycling pelotons: New insights by CFD simulation and wind tunnel testing*, Journal of Wind Engineering and Industrial Aerodynamics, Volume 179, Pages 319-337, 2018

[6] Gan E, Fong M, and Ng YL, *CFD Analysis of Slipstreaming and Side Drafting Techniques Concerning Aerodynamic Drag in NASCAR Racing*, CFD Letters, Volume 12, 2020.

[7] Chatard JC & Wilson B, *Drafting Distance in swimming*, Med. Sci. Sports Exerc., Volume 35, Pages 1176–1181, 2003.

[8] Coast JR & Piatt CA, *Heart Rate and Lactate Responses to Swimming in Various Drafting positions*,Journal of Swimming Research, Volume 15, Pages 27-30, 2001.

[9] Janssen M, Wilson BD, and Toussaint HM, *Effects of Drafting on Hydrodynamic and Metabolic Responses in Front Crawl Swimming*, Med. Sci. Sports Exerc., Volume 41, Pages 837–843, 2009.

[10] Borg GAV, *Psychophysical bases of perceived exertion.* Med. Sci. Sports Exerc., Volume 14(5), Pages 377–381, 1982. https://doi.org/10.1249/00005768-198205000-00012

[11] Silva AJ, Rouboa A, Moreira A, Reis VM, Alves F, Vilas-Boas JP & Marinho DA, *Analysis of drafting effects in swimming using computational fluid dynamics*, Journal of Sports Science and Medicine, Volume 7, Pages 60-66, 2008

[12] Marinho DA, Reis VM, Alves F, Vilas-Boas JP, Machado L, Silva AJ & Rouboa A, *Hydrodynamic Drag During Gliding in Swimming*, Journal of the Royal Society Interface, 2019

[13] Yuan ZM, Li M, Ji CY, Li L, Jia L, Incecik A, *Steady hydrodynamic interaction between human swimmers*, Journal of Applied Biomechanics, Volume 25, Pages 253-257, 2009

[14] Westerweel J, Aslan K, Pennings P, Yilmaz B, *Advantage of a lead swimmer in drafting*, 2016, arXiv:1610.10082v1

[15] MIT, Marine Hydrodynamics, *Water waves*, https://web.mit.edu/13.021/demos/lectures/lecture19.pdf

[16] See supplementary material at [URL will be inserted by publisher] for the .stl of the model's geometry.

[17] Phyling, Drahi-X-Novation Center, https://www.phyling.fr/

[18] OpenFoam, 2022, https://openfoam.org/

[19] OpenFoam, UserGuide v2112, *k-omega Shear Stress Transport (SST)*, https://www.openfoam.com/documentation/guides/latest/doc/guide-turbulence-ras-k-omega-sst.html